Electronic Supplementary Material (ESI) for Nanoscale.
This journal is © The Royal Society of Chemistry 2024

Electronic Supplementary Material

Insight into the transport of salt of moderated solubility through nanochannels: negative incremental resistance assisted by geometry

Gregorio Laucirica,[1†] L. Miguel Hernández Parra,[1] Ángel Luciano Huamani,[1] Michael F. Wagner,[2] Alberto G. Albesa,[1] María Eugenia Toimil-Molares,[2,3] Waldemar Marmisollé [1] and Omar Azzaroni [1]

1. Instituto de Investigaciones Fisicoquímicas Teóricas y Aplicadas (INIFTA), Departamento de Química, Facultad de Ciencias Exactas, Universidad Nacional de La Plata, CONICET, CC 16 Suc. 4, La Plata B1904DPI, Argentina.

2. GSI Helmholtzzentrum für Schwerionenforschung, 64291, Darmstadt, Germany.

3. Technische Universität Darmstadt, Materialwissenschaft, 64287, Darmstadt, Germany.

[†] Current affiliation: UCAM-SENS, Universidad Católica San Antonio de Murcia, UCAM HiTech, 30107 Murcia, Spain.

1. SEM characterization

The different channels employed in the main article were characterized by scanning electron microscopy (SEM) analysis (Zeiss Gemini 500 field-emission electron microscope) (**Figure S1**). For this, multi-channel membranes (10^6 channels per cm^2) were etched in the same conditions as those single-pore membranes used during the ion transport experiments. For top-view images, a thin gold layer was deposited onto the membrane surface by gold sputtering to diminish charging effects. Results are available in **Table S1**.

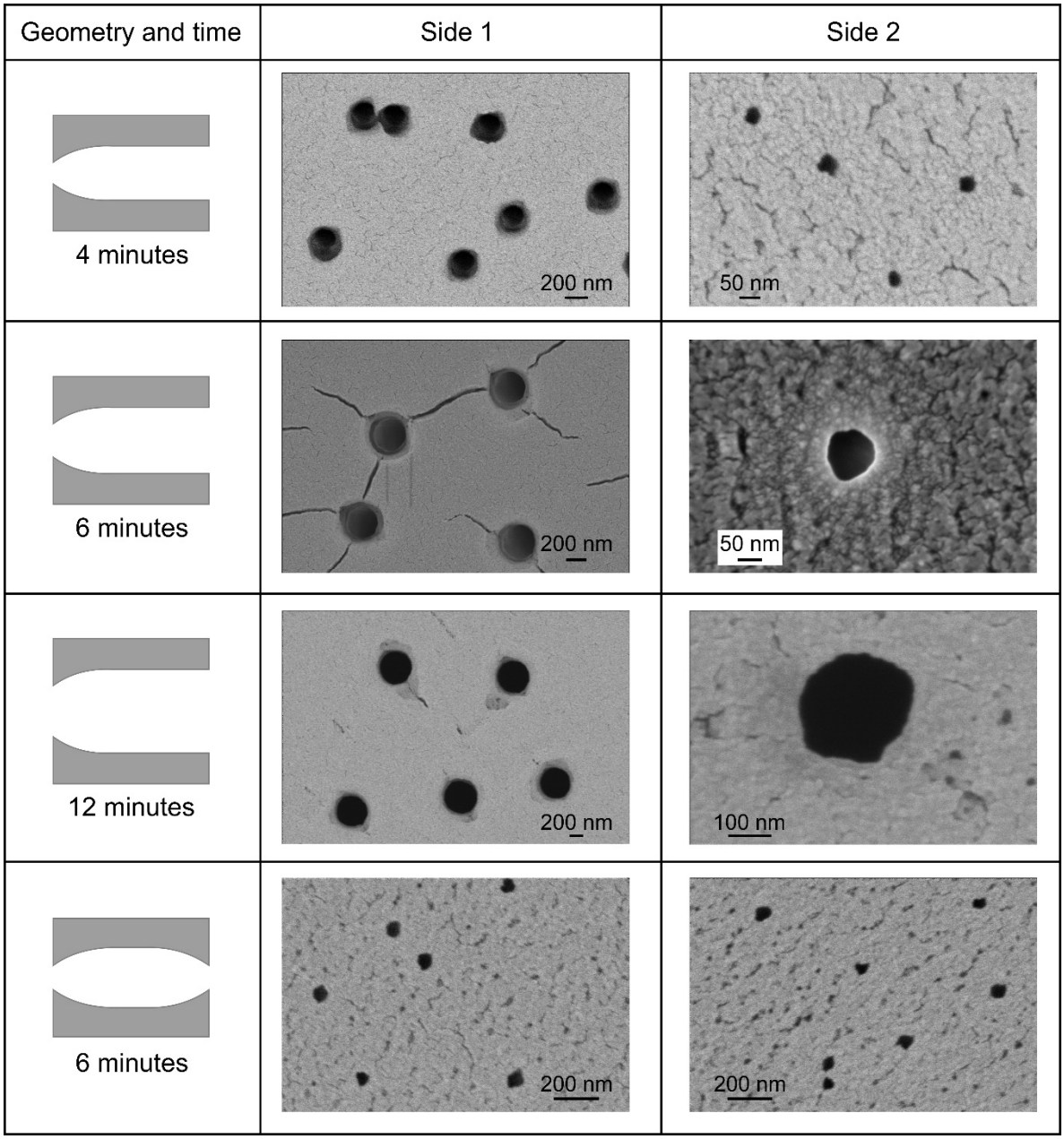

Figure S1. Top-view SEM images for the different samples employed in the main article.

Table S1. Size obtained from the SEM analysis for the different samples.

Etching time / min	Geometry	Side 1 size / nm	Side 2 size / nm
4	Bullet	62 ± 20	258 ± 19
6	Bullet	100 ± 8	357 ± 17
12	Bullet	237 ± 17	443 ± 14
6	Cigar	69 ± 5	70 ± 6

Cross-section images were analyzed via SEM for samples etched for 6 minutes to demonstrate the prevalence of bullet- and cigar-shaped geometries when etching is performed in the presence of Dowfax 2a1 surfactant. For this, the multichannel membranes were broken and measured at 90°. To break the membrane without losing the geometrical features of the channel, the samples were exposed to 72 hours of UV light irradiation and then they were broken inside liquid nitrogen by pressing against a surface.

For the bullet-shaped channels, the cross-section images show a narrow aperture with a parabolic profile (so-called tip) on the side 1 and a wide aperture with a cylindrical profile (so-called base) on the side 2. Instead, for the cigar-shaped channels, both sides show narrow apertures with parabolic profiles.

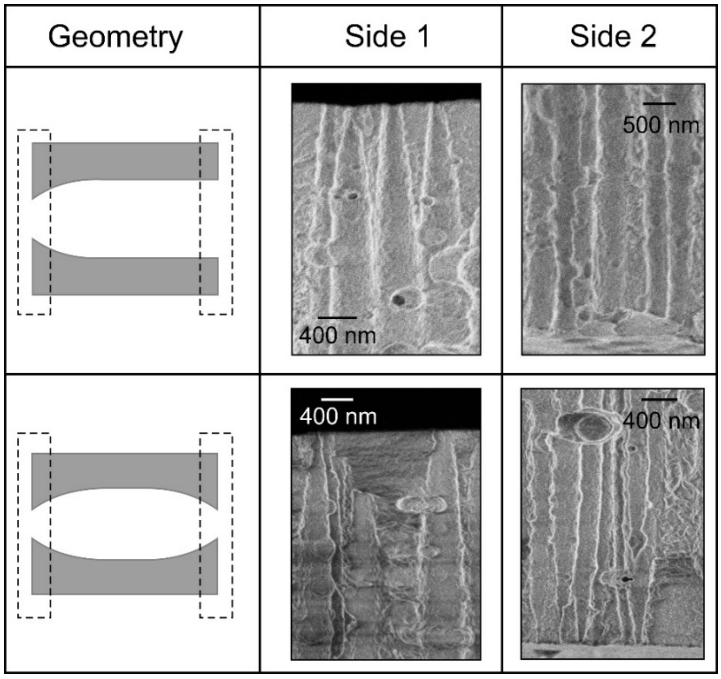

Figure S2. Cross-section SEM images for the channels with bullet-shaped and cigar-shaped geometries.

2. Iontronic output in different supporting electrolytes

To test the hypothesis of salt precipitation, I-V curves were recorded using alternative supporting electrolytes such as KCl and $NaClO_4$. **Figure S3(a)** illustrates that when ClO_4^- is replaced with

Cl^- to form a soluble salt like KCl, the iontronic output exhibits the expected rectifying behavior in a bullet-shaped nanochannel. Similarly, when K^+ is substituted with Na^+ to form a soluble salt like $NaClO_4$, the iontronic output again displays typical rectifying behavior without NIR events (**Figure S3(c)**). Hence, these experiments indicate that the presence of both ions K^+ and ClO_4^- is necessary to observe the NIR event, which reinforces the hypothesis of a phenomenon explained by salt precipitation (**Figure S3(b)**).

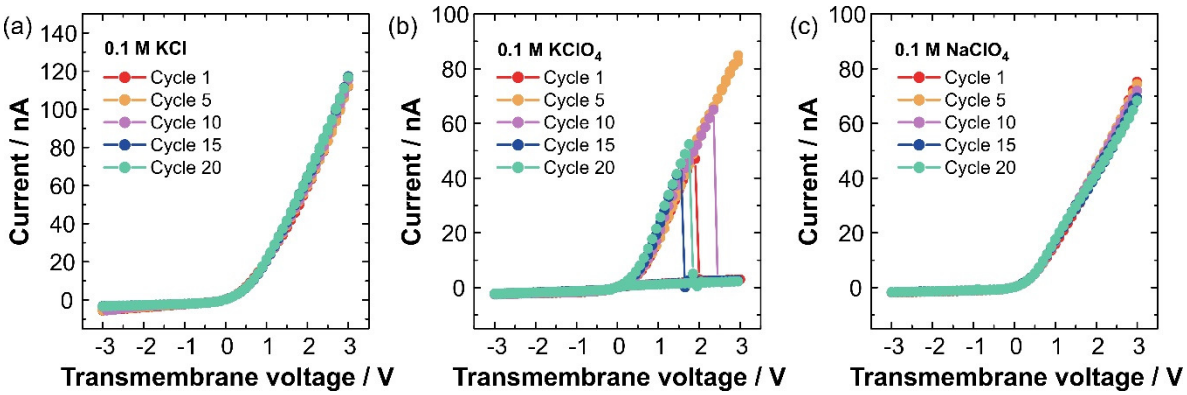

Figure S3. I-V curves obtained using different supporting electrolytes: (a) KCl, (b) $KClO_4$, and (c) $NaClO_4$. All measurements were conducted at pH 6.

3. Iontronic output in different $KClO_4$ concentrations

To gain insight into the formation of the precipitates, I-V curves were performed at different $KClO_4$ concentrations. As can be seen in **Figure S4**, NIR phenomena can be evidenced in both 0.01 M and 0.1 M $KClO_4$ measurements. The explanation is related to the high ion enrichment produced in both cases due to ion selectivity and rectification behavior. However, unlike the measurements taken in 0.1 M $KClO_4$, the iontronic output recorded in 0.01 M $KClO_4$ exhibits a significant degree of instability, which makes it difficult to obtain three stable conductance states and high NIR ratios. For this reason, 0.1 M $KClO_4$ solutions were employed throughout the article.

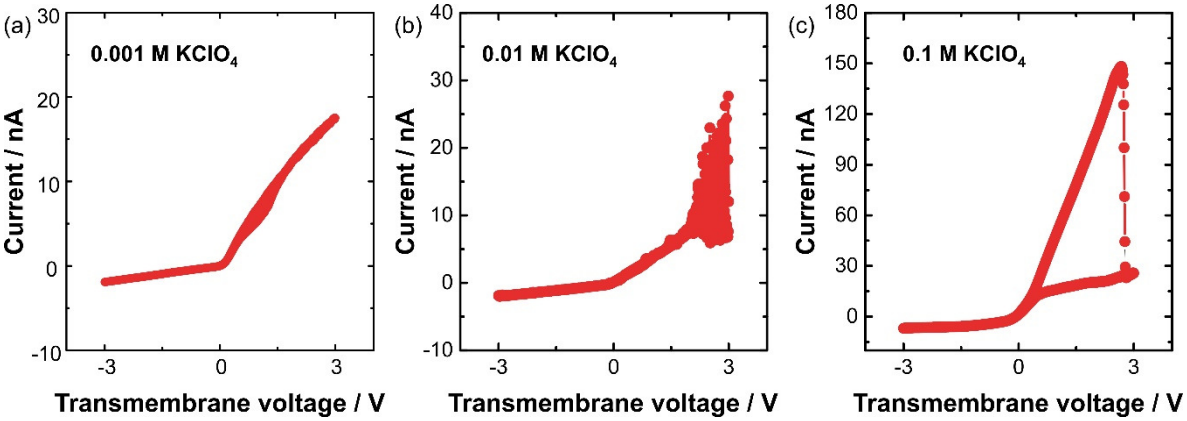

Figure S4. I-V curves recorded at different $KClO_4$ concentrations: (a) 0.001 M, (b) 0.010 M, and (c) 0.1 M. All measurements were conducted at pH 6.

4. Iontronic output in KCl at different pH conditions

Chemical etching of PET irradiated membranes exposes carboxylic groups on the channel surface. Depending on the pH conditions, carboxylic groups can be deprotonated to generate negatively charged carboxylate groups. The presence of a charged surface in asymmetric channels such as bullet-shaped and conical channels gives rise to a rectifying behavior where the efficiency of the diode-like behavior (quantified by the rectification factor) provides qualitative information on the magnitude and type of surface charge. **Figure S5** shows the rectification factors obtained for the bullet-shaped channel (6 minutes of etching) in 0.1 M KCl at different pH conditions. As can be seen, the f_{rec} is maximized at alkaline conditions which is attributed to the increment in the surface charge due to the high degree of deprotonated carboxylate groups.

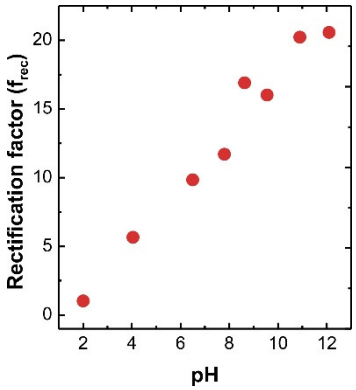

Figure S5. Rectification factors at different pH conditions. All the measurements were conducted in 0.1 M KCl employing a bullet-shaped channel (6 minutes of etching).

5. Reproducibility

Given the wide variability observed for the sample measured at pH 6, **Figure S6** presents the V_{thres} and NIR ratios obtained for five independent samples fabricated (6 minutes of etching) and tested (0.1 M $KClO_4$ at pH 6) under the same conditions. Considering all the samples with their corresponding 20 cycles, V_{thres} and NIR ratio averages of 1.7 ± 0.5 and 20 ± 7, respectively.

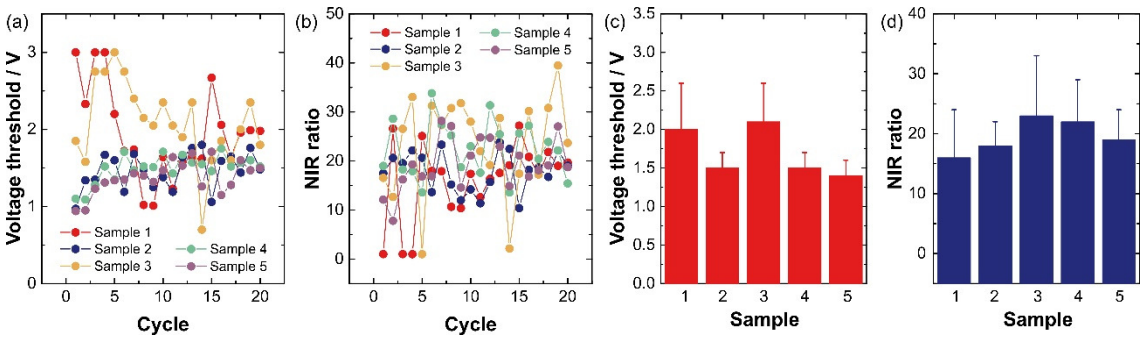

Figure S6. (a) Variations in V_{thres} and (b) NIR ratios across multiple voltammetric cycles for five independent samples. Each sample corresponds to membranes subjected to 6 minutes of etching, resulting in an approximate tip diameter of 100 nm. (c) Average V_{thres} and (d) NIR ratio values obtained from the five samples over 20 cycles. Bars correspond to the standard deviations of 20 voltammetric cycles. All measurements were performed in 0.1 M $KClO_4$ at pH 6.

6. Iontronic output of the different channels

Considering that the enrichment degree depends on the channel size, the iontronic output was evaluated for bullet-shaped of different aperture diameters. For this, the etching time during the nanofabrication varied between 4, 6, and 12 minutes. **Figure S7** shows the I-V curves in the presence of 0.1 M KCl (**(a)-(c)**) and 0.1 M $KClO_4$ for the three channels (**(d)-(f)**).

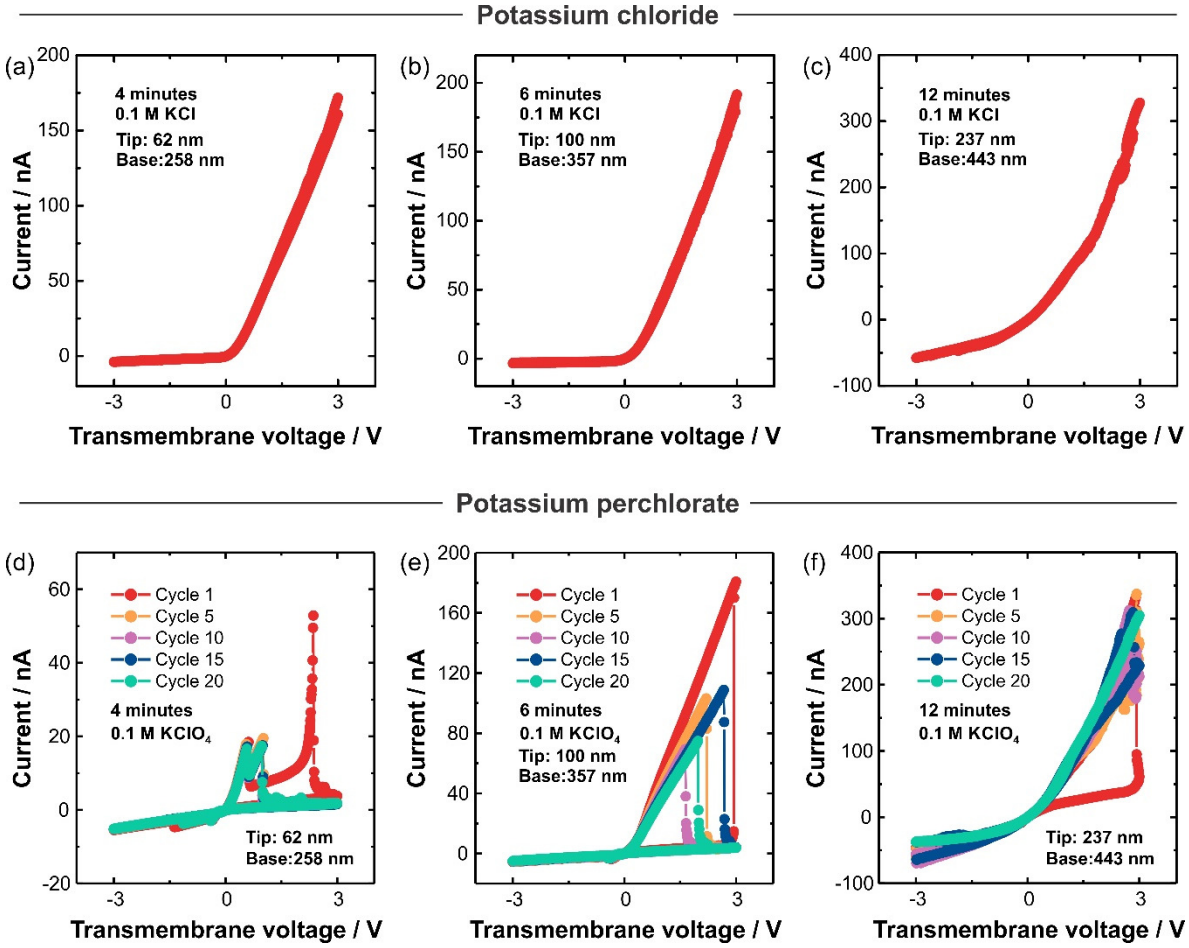

Figure S7. I-V curves in the presence of 0.1 M (a)-(c) KCl and (d)-(f) $KClO_4$ for the three different bullet-shaped channels. All the measurements were conducted at pH 6.

7. Iontronic output of a cylindrical channel

To discard a possible size effect in the results shown in the main text, the results in a cylindrical nanochannel with a diameter of 35 nm were reproduced in a cylindrical microchannel with a diameter of 240 nm (**Figure S8**). Similar to the results displayed by the 35 nm-nanochannel, the iontronic output for the microchannel in the presence of 0.1 M $KClO_4$ exhibits the typical ohmic behavior without NIR events.

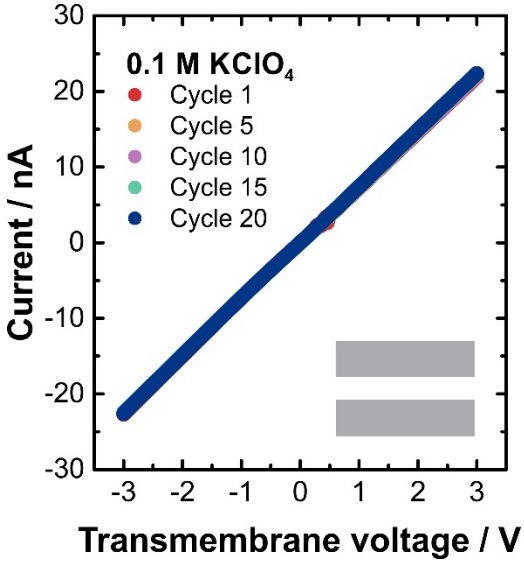

Figure S8. I-V curve in 0.1 M $KClO_4$ at pH 6 for a cylindrical channel of 240 nm in diameter.

8. Poisson-Nernst-Planck simulations

Results obtained from simulations based on the Poisson-Nernst-Planck equations were used to reinforce the hypothesis of salt precipitation as the main reason to explain the presence of NIR events in the I-V curves conducted in $KClO_4$ solutions. The model employed together with their assumptions and methodology has been addressed in detail elsewhere.[1]

The experimental I-V curves obtained in the presence of KCl at pH 6 were replicated through PNP simulations to identify nanochannels exhibiting analogous behaviors. After determining the representative channels for each geometry, predictions for ion profiles were made for experiments conducted using $KClO_4$ at different V_t values, as shown in **Figure S9**.

The experimental I-V curves for the bullet-shaped channel agree with the model constituted by a channel with tip and base diameters around 60 nm and 700 nm, respectively. Furthermore, the curvature parameter L/h was fixed in 16. For the cigar-shaped channel, the apertures were 55 nm and 38 nm with a lumen of 220 nm and, the curvature parameters L/h were fixed in 16 and 4. For the cylindrical channel, the diameter was 45 nm. For the analysis in of the channel size (Figure 5 in the main article), all the channel parameters were maintained except of the tip or aperture diameters.

The analysis of the ion distributions at the different V_t provides valuable information to rationalize the trend observed in the main article. In the case of the bullet-shaped channel, the concentrations of both cations and anions within most segments of the channel experienced enrichment for $V_t >$ 0 V and depletion for $V_t < 0$ V (**Figure S9(a)(i)-(ii)**). For both polarities of V_t, the concentration of K^+ ions exceeded that of ClO_4^- which can be attributed to the permselective nature of bare PET (**Figure S9(a)(iii)**). Notably, in the tip region (x=0 μm), K^+ ions are accumulated, while ClO_4^- ions are depleted due to the electrostatic interaction between mobile ions and the fixed surface charge at the tip.

For cigar-shaped nanochannels, the scenario is quite different. The K^+ ions tend to accumulate predominantly at both channel entrances but are depleted in the central region of the channel (**Figure S9(b)(i)**). This trend becomes more pronounced as V_t becomes more positive. Conversely, ClO_4^- ions are primarily depleted within the channel and at both apertures for most of the V_t values considered (**Figure S9(b)(ii)**). Only under negative V_t conditions, ClO_4^- ions displayed slightly higher concentrations than the bulk solution at one of the channel entrances. However, it is important to note that the degree of enrichment in this particular case is quite minimal, specially, compared to the bullet-shaped case (**Figure S9(b)(iii)**).

For cylindrical shape, the K^+ ions are accumulated inside the channel due to the negative surface charges (**Figure S9(c)(i)**). For its part, the ClO_4^- concentration is diminished compared to the bulk value (**Figure S9(c)(ii)**).

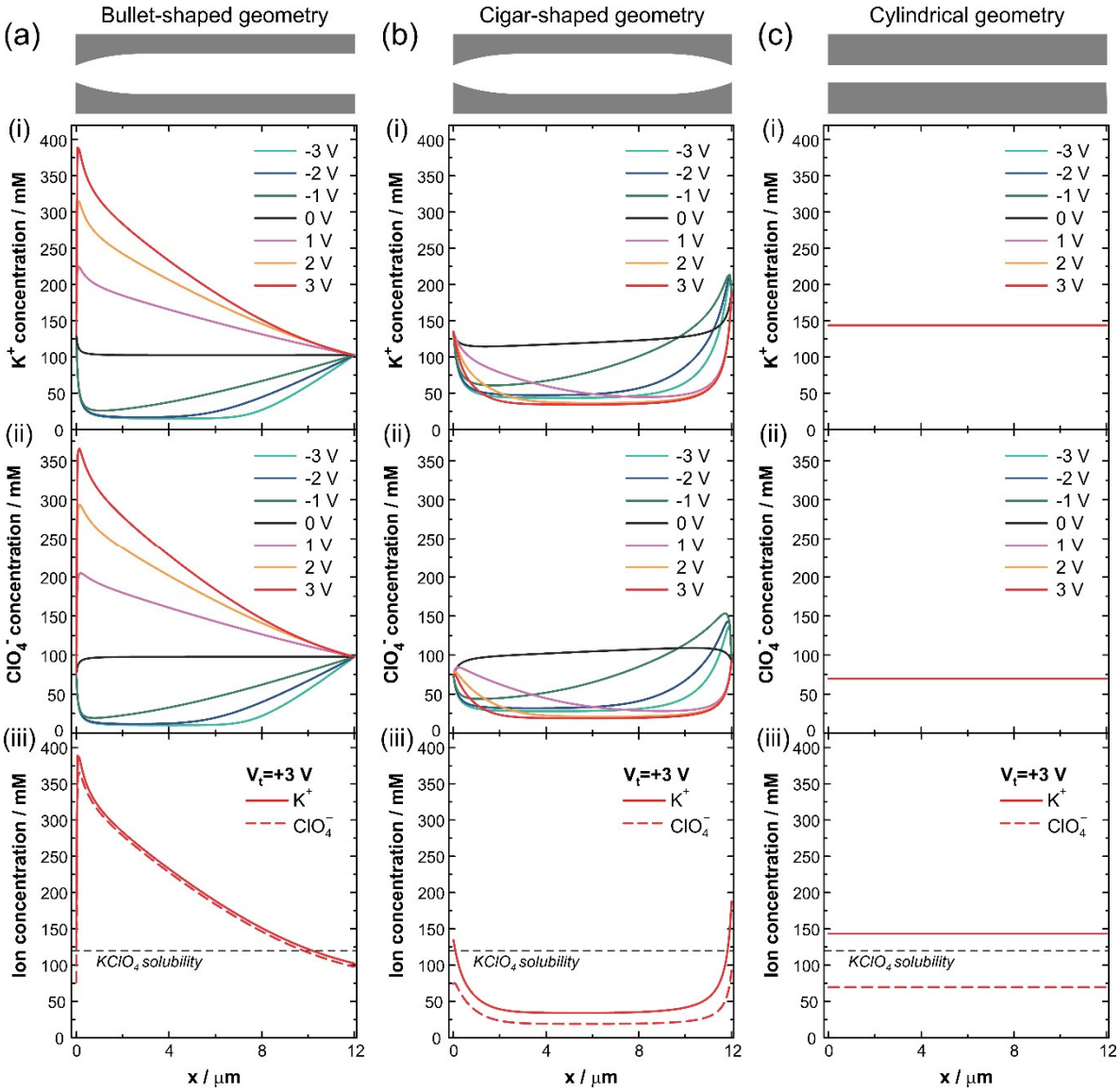

Figure S9. Ion profiles obtained by PNP simulations (surface charge 0.5 e/nm^2 -e: electron charge-). Arrows (a), (b), and (c) show the ion distributions obtained with bullet-shaped, cigar-shaped, and cylindrical channels, respectively. In all the cases, plots (i) and (ii) exhibit the potassium and perchlorate concentrations, respectively, in terms of the axial coordinate of the channel x at different V_t. For its part, figures (iii) showcase the potassium and perchlorate concentration in terms of the x-coordinate at V_t=+3 V.

Dashed lines indicate the salt solubility at 20°C.[2] x=0 µm and x=12 µm correspond to the channel entrances. For the case of the bullet-shaped channel, the tip is placed at x=0 µm. Plots in Figure S8(c)(i)-(ii) presents a high degree of overlapping that difficult to differentiate each other.

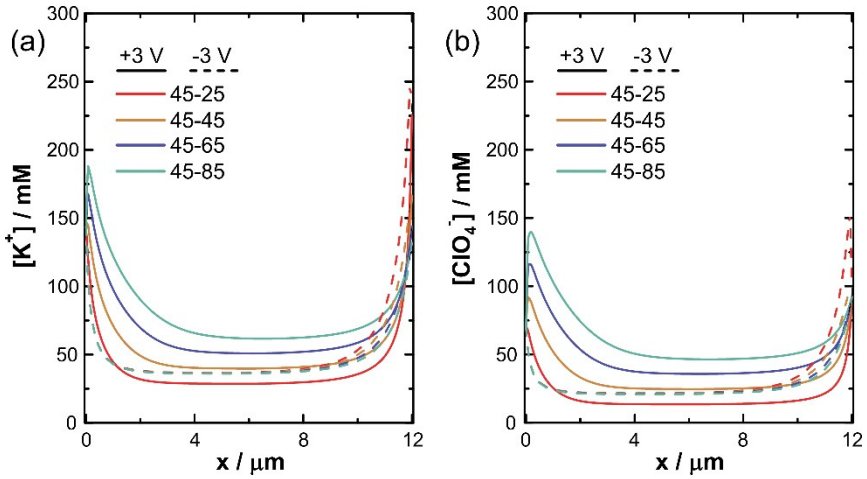

Figure S10. (a) Cation and (b) anion concentration profiles for cigar-shaped channels with different aperture diameters at both sides. First value of the legend corresponds to the channel diameter in nm for the aperture placed in x=0, while the second value corresponds to the diameter for the aperture in x= 12µm.

9. References

1 G. Pérez-Mitta, A. G. Albesa, M. E. Toimil-Molares, C. Trautmann and O. Azzaroni, *ChemPhysChem*, 2016, **17**, 2718–2725.

2 D. R. Lide, *CRC Handbook of Chemistry and Physics*, 90th Editi., 2010.